Received: 29 May 2024 | Revised: 26 July 2024 | Accepted: 31 July 2024

DOI: 10.1111/jace.20102

Journal of the American Ceramic Society

RESEARCH ARTICLE

Dissolution kinetics of cementitious magnesium silicate hydrate in air-equilibrated water

Abdul Wahab[1] | **Trinh Thao My Nguyen**[2] | **Dylan Singh**[1] | **Erika La Plante**[2]

[1]Department of Materials Science and Engineering, University of Texas at Arlington, Arlington, Texas, USA

[2]Department of Materials Science and Engineering, University of California, Davis, Davis, California, USA

Correspondence
Erika La Plante, Department of Materials Science and Engineering, University of California, Davis, Davis, CA 95616, USA.
Email: eclaplante@ucdavis.edu

Funding information
National Science Foundation, Grant/Award Number: #2342381

Abstract

Magnesium silicate hydrate (M-S-H) represents a promising alternative to traditional cement, particularly for low-pH construction applications such as nuclear waste encapsulation and carbon dioxide injection. The durability of construction materials, a critical aspect of their suitability for various purposes, is primarily governed by the kinetics of dissolution of the binder phase under service conditions. In this study, we employed in situ atomic force microscopy to assess the dissolution rates of M-S-H in water equilibrated with air. Quantitative analysis based on changes in volume and height revealed dissolution rates ranging from 0.18 to 3.09×10^{-12} mol/cm^2/s depending on the precipitate Mg/Si ratio and morphology. This rate surpasses its crystalline analogs, talc ($Mg_3Si_4O_{10}(OH)_2$) and serpentine ($Mg_3(Si_2O_5)(OH)_4$), by about three to five orders of magnitude. Interestingly, oriented M-S-H dissolved faster than non-oriented M-S-H. Spatially resolved assessments of dissolution rates facilitated a direct correlation between rates and morphology, showing that edges and smaller crystallites dissolve at a faster pace compared to facets and larger crystallites. The outcomes of this study provide insights into the mechanisms governing the dissolution of M-S-H and the factors dictating its durability. These findings hold implications for the strategic design and optimization of M-S-H for various applications.

KEYWORDS

atomic force microscopy, dissolution rate map, non-classical growth, oriented precipitates, time series

1 | INTRODUCTION

The demand for concrete is anticipated to continue growing in the future, with concerns arising from the low durability and relatively short lifespans of many concrete structures.[1] These issues not only pose technical and economic challenges but also raise sustainability concerns.[2] The rate of concrete deterioration is influenced by various factors including composition, curing conditions, and environmental exposure during the structure's service life.[3] Significantly, degradation primarily stems from the dissolution of the binder, which increases porosity and permeability. Hence, materials with low dissolution rates tend to exhibit enhanced durability and longer lifespans, whereas those with high dissolution rates may necessitate frequent maintenance or replacement.[4]

Magnesium silicate hydrates (M-S-H) hold promise as a low-pH cement suitable for various applications, including nuclear waste management.[5] Lower pH cements, such as M-S-H, demonstrate improved compatibility with clay barriers,[6] whose neutral pH can lead to the dissolution of typical ordinary Portland cement binder that is composed

of calcium silicate hydrate (C-S-H). M-S-H exhibits low crystallinity and a layered structure reminiscent of clay minerals with a high degree of polymerization in the silica network.[7] Tetrahedral sites within M-S-H are often bound with two or three neighbors, characterized as Q^2 and Q^3 species.[7] Although the precise structure of M-S-H remains incompletely understood, analytical techniques such as Raman spectroscopy, Si-nuclear magnetic resonance (NMR), and X-ray diffraction suggest that M-S-H with Mg/Si ratios between 0.8 and 1.0 resembles disordered talc ($3MgO{\cdot}4SiO_2{\cdot}H_2O$),[8] whereas higher Mg/Si ratios are associated with serpentine-like structures such as lizardite ($3MgO{\cdot}2SiO_2{\cdot}2H_2O$).[9,10] M-S-H exhibits a variable composition, typically with a molar Mg/Si ratio ranging from 0.5 to 1.5. At Mg/Si ratios of 0.5-0.7, excess Si may be present as amorphous silica (SiO_2), whereas at ratios of 1.0–1.5, excess Mg may exist as brucite ($Mg(OH)_2$).[7,11] Our previous study has shown that increasing the Mg/Si ratio in the solid phase leads to the depolymerization of silica tetrahedra within M-S-H, with only minor amounts of co-precipitated brucite and silica, if any.[12] However, the implications of this depolymerization on the deteriorative properties of M-S-H are not yet fully understood.

In this study, we quantified the dissolution rate of M-S-H in deionized (DI) water using in situ atomic force microscopy (AFM). In situ AFM enables high-resolution surface topography-based measurement of dissolution rates under controlled environmental conditions. The findings from this study offer valuable insights into the selection and design of alternative cementitious materials aimed at ensuring long-lasting performance.

2 | METHODS

2.1 | Sample preparation and characterization

The experimental procedure employed in this study is illustrated in Figure 1. The growth solution for the synthesis of M-S-H was prepared by mixing stock solutions of sodium metasilicate pentahydrate ($Na_2SiO_3{\cdot}5H_2O$, 99% purity) and magnesium nitrate hexahydrate ($Mg(NO_3)_2{\cdot}6H_2O$, ≥95% purity) in ultrapure DI water (Milli-Q, ≥18.20 MΩ·cm) in a polypropylene centrifuge tube to achieve the desired [Mg]/[Si] molar ratios of 0.5:1, 1:1, and 1.5:1 (Table 1).[12] Our previous study has shown that synthesized M-S-H has a composition that generally matches the growth solution composition.[12] A single crystal mica disc (Ted Pella, V1) was submerged in the centrifuge tubes to allow the growth of M-S-H on the mica (001) surface. Subsequently, the tubes were sealed and stored at ambient temperature (23 ± 2°C) for about 120 min (Table 1). The mica discs were removed from the centrifuge tube using tweezers and then dried using ultra-high purity nitrogen gas. The samples were stored under ambient conditions before dissolution rate measurements were conducted.

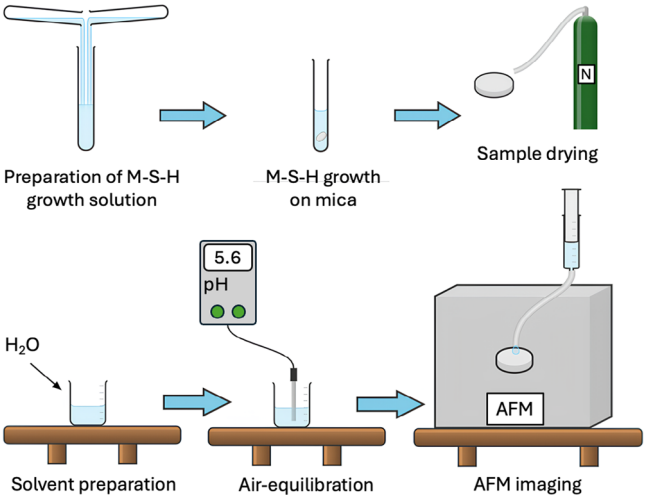

FIGURE 1 Schematic showing the experimental procedure employed in this study. M-S-H, magnesium silicate hydrate.

2.2 | Dissolution rate

Before dissolution, water was equilibrated with atmospheric CO_2 (approximate pCO_2 of $10^{-3.4}$) by allowing the container to stand openly in the ambient laboratory environment for at least 2 days, covered with a Kimwipe to prevent contamination (Figure 1). Precipitates of M-S-H on mica were dissolved in air-equilibrated ultrapure DI water. At the beginning of each experiment, 200 µL of DI water was injected into the fluid cell at a flow rate of 5 µL/s. The flow was stopped and the topography of the overgrowth films was characterized in situ (i.e., while the sample is exposed to water) using an Asylum Research Cypher ES Environmental AFM operating in AC mode fitted with an integrated fluid cell with inlet and outlet gas and liquid ports, at a controlled temperature of 25.0 ± 0.1°C.[13] A monolithic silicon probe with a nominal force constant of 3 N/m, resonance frequency of 75 kHz, tip radius < 10 nm, length of 225 µm, width of 28 µm, and thickness of 3 µm was used. Image processing and analysis were performed using Gwyddion[14] and limited to first-order flattening (planar slope correction).

The dissolution rates were measured by observing the changes in the M-S-H surface topography relative to the mica surface, which has a dissolution rate of $9.4 \pm 0.26 \times 10^{-16}$ mol/cm^2/s at a pH of 6.1,[15] estimated to be ~3 to 4 orders of magnitude slower than M-S-H. Indeed, there was no indication of mica dissolution, which

TABLE 1 Experimental conditions for M-S-H dissolution at different molar ratios of [Mg]/[Si] (0.5, 1.0, and 1.5).

[Mg]/[Si]	[Mg] (mM)	[Si] (mM)	pH (initial)	Time (min)	T (°C)
0.5	50	100	–	100	25.0
0.5	50	100	5.93	121	25.0
0.5	50	100	5.88	119	25.0
1.0	100	100	6.05	129	25.0
1.0	100	100	5.41	154	25.0
1.5	75	50	6.07	125	25.0
1.5	75	50	5.73	122	25.0
1.5	75	50	5.21	121	25.0

Note: Reported are the concentrations of Mg and Si in the growth solutions and corresponding [Mg]/[Si] ratios, initial pH of atmospheric CO_2-equilibrated water before dissolution reaction, total dissolution time, and dissolution temperature.
Abbreviation: M-S-H, magnesium silicate hydrate.

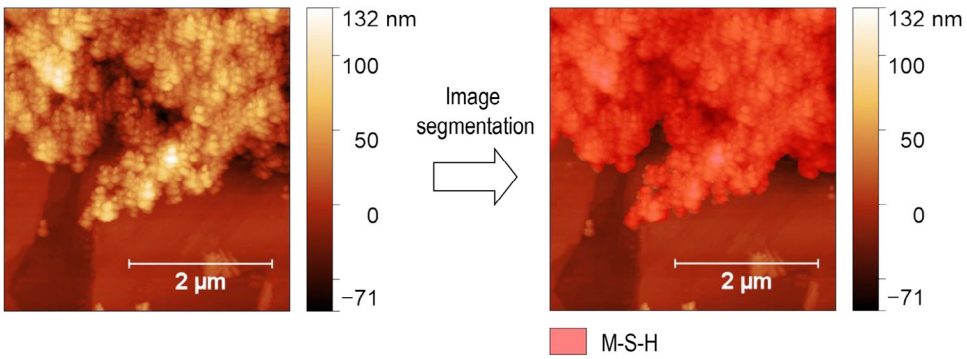

FIGURE 2 A representative atomic force microscopy (AFM) image illustrating the segmentation procedure. To determine the average height, surface area, and volume of magnesium silicate hydrate (M-S-H) precipitates, a mask was carefully created in Gwyddion[14] for each image in the time series.

allowed for the correction of images for temporal drift by cropping mutually corresponding areas in two or more images. Image segmentation was performed to delineate pixels corresponding to M-S-H from those corresponding to mica (Figure 2). Given the limitations of built-in segmentation algorithms in Gwyddion,[14] a manual image segmentation approach was adopted. Specifically, masks were manually drawn around M-S-H precipitates for each image using the "Mask Editor" tool in Gwyddion.[14] This approach ensured that all precipitates were included in the analysis. For time series analyses, particular attention was paid to image alignment to correct for any drift and ensure consistency in the masked regions across the series. Distinct surface features on the mica substrate were used as reference points for alignment using the "Align Scans" tool. Therefore, the data consisted of measurements taken at selected intervals during the experiment to quantify the changes in height, surface area, and volume over time.

Dissolution rates were obtained from either volume change or height change of the precipitates. For volume-based dissolution rates, the total volume of M-S-H is converted to moles using its molar volume, taken as 189.8 cm^3/mol for the composition $3MgO{\bullet}4SiO_2{\bullet}5H_2O$.[16] The calculated moles are normalized to the surface area, and a linear equation was fitted to the surface area-normalized volume over time to obtain the dissolution rate in units of mol/cm^2/s. The height-based dissolution rate was determined using a method outlined previously wherein the slope describing the change in average height over time is normalized to the molar volume.[17]

3 | RESULTS AND DISCUSSION

3.1 | Dissolution rates of M-S-H and comparison with analogous silicate minerals

The experimental conditions are summarized in Table 1. The pH of the CO_2-equilibrated water calculated using the geochemical modeling software, PHREEQC,[18] is 5.6. As depicted in Table 1, the initial pH values of the CO_2-

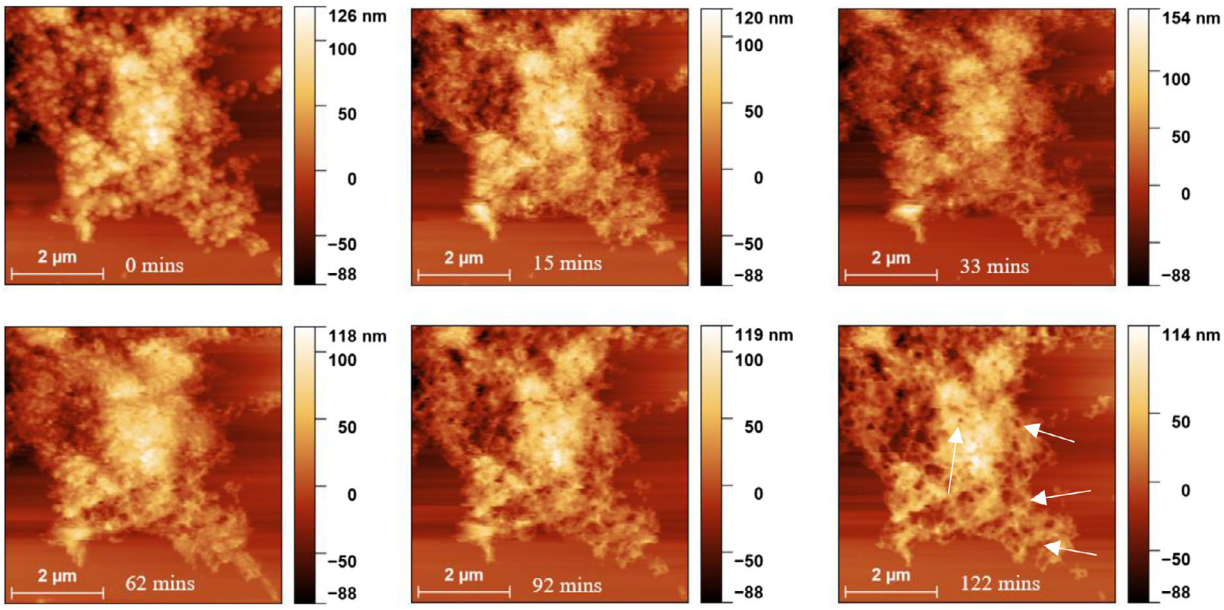

FIGURE 3 AFM images showing M-S-H ([Mg]/[Si] = 1.5) on a mica substrate reacted with air-equilibrated water, illustrating the progressive dissolution of M-S-H. The formation of etch pit-like features, as well as the predominant dissolution near edges, is evident (white arrows).

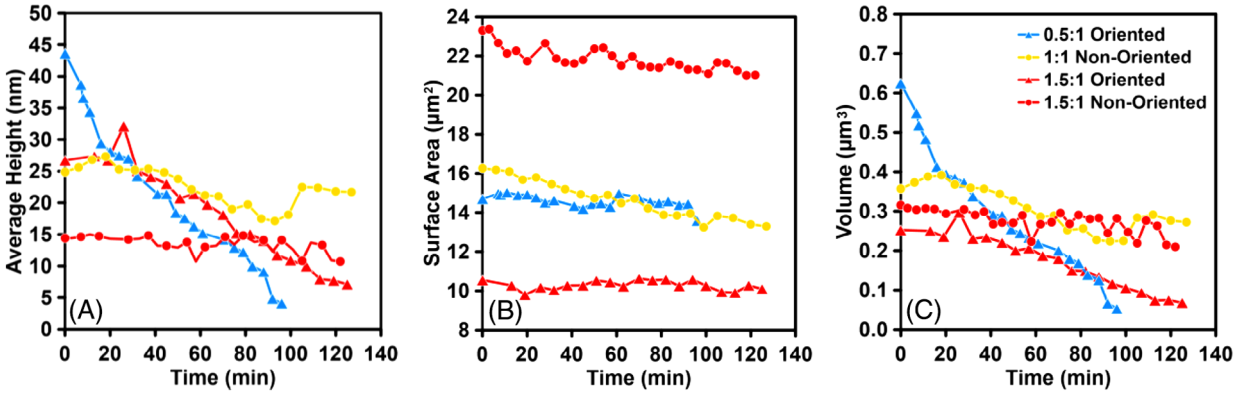

FIGURE 4 Evolution of (A) average height, (B) surface area, and (C) volume obtained from time series AFM images for different [Mg]/[Si] ratios and morphologies. Initial (i.e., $t = 0$) images are collected in air, that is, prior to the introduction of water in the fluid cell. The results show near-linear decreases in average height and volume over time.

equilibrated water varied but remained consistently close to the anticipated value.

Representative time-series AFM images illustrating the dissolving M-S-H on mica are shown in Figure 3. Two types of morphologies are observed: non-oriented and oriented, which are further discussed in Section 3.2. The dissolution rates remain near-constant throughout the entire experimental duration (Figure 4), suggesting that despite the lack of convective flow, the solution remained highly undersaturated with respect to the dissolving phase.[19,20] Similar experimental conditions have been employed using semi-stagnant DI water in the AFM fluid cell for studying calcite ($CaCO_3$) dissolution, with water refreshed every 5 or 10 min, wherein the formation of etch pits indicates a highly undersaturated reacting fluid.[21] The formation of etch pit-like features, which increased in both size and number over time, was also observed in this study (Figure 3). Furthermore, it has been proposed that minerals with slow dissolution rates, less than approximately 1.6×10^{-10} mol/cm^2/s (estimated from the given data) are generally surface reaction-controlled.[22] Finally, the persistence of highly undersaturated conditions is also supported by geochemical modeling of the reaction solution using data from Figure 4.

TABLE 2 Dissolution rates of M-S-H measured at various Mg/Si ratios. The uncertainties represent the standard errors obtained from linear regression.

Mg/Si	Morphology	Dissolution rate based on volume change ($\times 10^{-12}$ mol/cm^2/s)	Dissolution rate based on height change ($\times 10^{-12}$ mol/cm^2/s)
0.5	Oriented	2.93 ± 0.14	3.09 ± 0.14
1.0	Non-oriented	0.39 ± 0.10	0.50 ± 0.11
1.5	Non-oriented	0.17 ± 0.04	0.18 ± 0.05
	Oriented	1.53 ± 0.10	1.72 ± 0.10

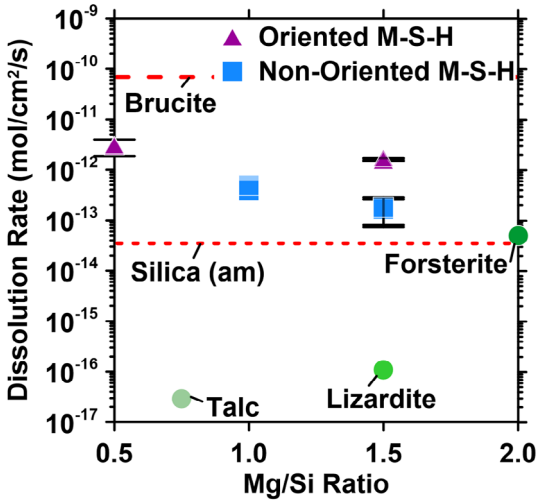

FIGURE 5 Dissolution rates of M-S-H measured in this study (light colors refer to height-based rates, and dark colors refer to volume-based rates, Table 2), talc at pH 4.06,[25] lizardite at pH 3.84,[26] forsterite at pH 5.4,[27,28] amorphous silica at pH 6.2,[29,30] and brucite near pH 5.6.[31] Increasing Mg/Si ratio correlates with increased dissolution rates for talc, lizardite, and other phyllosilicates under comparable pH conditions.

In single crystals, etch pits impact dissolution by increasing its reactive surface area. As etch pits form and expand, they create additional sites for dissolution reactions to occur. For instance, in quartz, etch pit densities as high as 10^{10} cm^{-2} have been reported, indicating a substantial increase in the reactive surface area.[23] Etch pits also expose high-energy sites on mineral surfaces, often associated with crystal defects or dislocations. These sites exhibit higher reactivity, compared to flat, defect-free surfaces, leading to localized areas of enhanced dissolution.

While distinct from true etch pits, analogous etch pit-like features are observed in M-S-H particulates (Figure 3). Similar to etch pits found in single crystals, these features indicate rapid localized dissolution, exposing edges that could contribute to an overall increase in dissolution rates.[23,24] Furthermore, rapid dissolution within these depressions could alter local solution chemistry and influence dissolution progression.[23] For M-S-H, this mechanism could lead to complex dissolution morphologies and spatial variation in rates. The development of etch pit-like features can also have implications for the long-term durability of M-S-H. The propagation of these features may weaken the material structure, potentially leading to increased susceptibility to further degradation or mechanical failure. Understanding these processes is crucial for predicting the long-term performance of M-S-H-based concrete.

The dissolution rates, quantified based on the data presented in Figure 4, are summarized in Table 2. To the best of our knowledge, these are the first quantifications of M-S-H dissolution rates. Both height-based and volume-based measurements yield similar results within experimental uncertainty. An apparent decrease in dissolution rates with rising [Mg]/[Si] ratio is evident (Figure 5). While the presence of secondary phases might explain the unexpected rate increase at low Mg/Si, it is noteworthy that the precipitation of brucite, which will tend to artificially increase rates, is more likely to occur at high, rather than low, Mg/Si ratios.[16] Nevertheless, it should be noted that these phases, if present, are not uniformly distributed, and the uneven distribution of associated phases could contribute to the observed disparity in dissolution rates. Alternatively, a higher concentration of amorphous silica at high Mg/Si may lead to decreased dissolution rates. This phenomenon is attributed to the immediate precipitation of M-S-H, which reduces the pH and subsequently promotes silica precipitation.[12] It is also worth noting that the observed variation in dissolution rates across Mg/Si ratios is similar to that across different morphologies for the same Mg/Si ratio (Table 2).

M-S-H possesses a semi-crystalline structure primarily composed of Q^2 and Q^3 species, with Q^3/Q^2 as indexed using both NMR and Fourier-transform infrared spectroscopy decreasing as Mg/Si ratios increase.[12,16] Q^3 species, characterized by greater polymerization, consequently demonstrate greater resistance to dissolution, compared to Q^2.[16] Similar to other silicates, the dissolution of semi-crystalline magnesium silicate, is driven by an ion-exchange reaction.[32,33] It is anticipated that dissolution initially occurs at surface defects, such as scratches or regions with high curvature, which typically harbor a higher concentration of undercoordinated and strained Q^2 groups.[32] As these sites become depleted, dissolution stabilizes, with new Q^2 groups continuously exposed at particle edges and areas where impurities have been removed.[32]

The dissolution rate of M-S-H is three to five orders of magnitude higher than that of talc and lizardite under

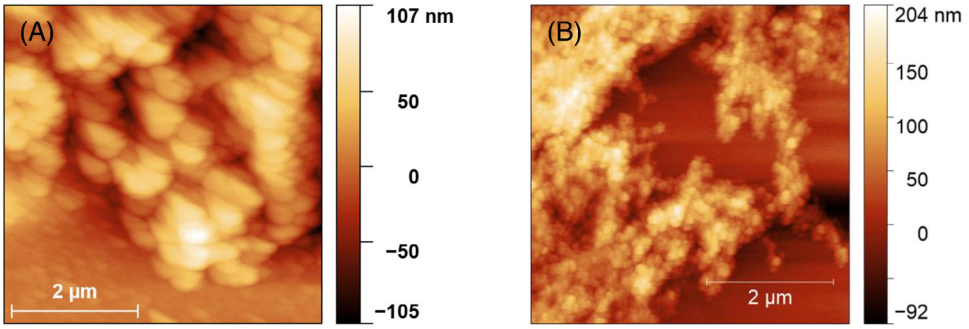

FIGURE 6 Height and amplitude images showing (A) oriented and (B) non-oriented morphologies of M-S-H grown from solutions with [Mg]/[Si] ratios of (A) 0.5 and (B) 1.5.

similar environmental conditions (Figure 5). Far-from equilibrium dissolution rates of lizardite at pH = 3.84 and talc at pH = 4.06 at near-ambient temperature are 1.1×10^{-16} mol/cm^2/s and 2.9×10^{-17} mol/cm^2/s.[25,26] These differences are consistent with the highly defective structure of M-S-H, compared to its crystalline analogs. In talc, magnesium is situated in octahedral positions linked by oxygen bridges to four silicon tetrahedra and two protons.[34] Since octahedral Mg–O bonds break faster than tetrahedral Si–O bonds, talc dissolution is initiated by the breaking of Mg–O bonds followed by the rapid removal of Mg atoms in Mg–H exchange reactions.[25] Similar to talc, M-S-H is composed of octahedral Mg–O and tetrahedral Si–O. Hydrolysis of the Si–O–Si and Si–O–Al bonds is usually considered the rate-limiting step of dissolution in clays,[35,36] consistent with Mg–O bonds breaking more rapidly than Si–O bonds.[33,37] Nonetheless, Si–O bonds can be weakened by breaking nearby bonds (e.g., Mg–O),[25] implying that the factors that affect Mg–O bond breaking also influence overall dissolution rates. Interestingly, M-S-H dissolution rates are closely aligned with dissolution rates of forsterite (Mg_2SiO_4) which is around 5×10^{-14} mol/cm^2/s at pH = 5.4 and pCO_2 = 0.5 atm, quantified from dissolved Mg concentrations.[27] Forsterite consists of isolated silica tetrahedra linked together by Mg^{2+} ions.[38]

3.2 | Influences of morphology on dissolution rates

M-S-H has a complex microstructure consisting of various morphologies that can contribute to variability in the dissolution rates. Spheroidal precipitates around 30 nm across in diameter are observed, which are either oriented or non-oriented (Figure 6). The oriented morphology often consists of elongated grains aligned in a particular direction (Figure 6A). In contrast, the non-oriented morphology is characterized by a mixture of spheroidal and irregularly shaped grains with no preferred alignment (Figure 6B). The aggregation of the small spheroidal particles further results in a range of secondary morphologies such as peaks, valleys, and other complex structures.

A link between the morphology and dissolution rate is observed (Figure 5). At a Mg/Si ratio of 1.5, oriented M-S-H dissolves almost 10 times faster than non-oriented M-S-H. This can be explained by the increased porosity in oriented M-S-H caused by inefficient packing as observed in other mesocrystalline structures that form by particle attachment.[39,40] Another potential reason for the increased dissolution rate of oriented particles is *dissolution by particle detachment*, which is characterized by neck formation in thin regions followed by particle break-up.[40] Additional studies are needed to ascertain the prevailing processes that are operative during M-S-H dissolution.

Height difference maps demonstrate spatial variation in dissolution rates (Figure 7). It is evident that hill and valley areas dissolve faster than planar areas (arrows in Figure 7). Over the examined dissolution period, near-complete dissolution of the fine satellite particulates was observed, while the larger central precipitates underwent partial dissolution (arrows in Figure 7A,B). Within the large aggregate, the grain edges preferentially dissolve, presumably because of the higher presence of reactive features like steps, kinks, and terraces, analogous to single crystals.[22]

3.3 | Comparison with C-S-H dissolution rates

The greater barrier for water exchange around Mg^{2+} ions than Ca^{2+} ions suggests that M-S-H is more resistant to dissolution and chemical alteration relative to C-S-H. Furthermore, M-S-H is more polymerized than C-S-H,[5] further suggesting greater aqueous stability of the former. Indeed, M-S-H is considerably more stable at low pH, compared to C-S-H, which is considered to be unstable at pH

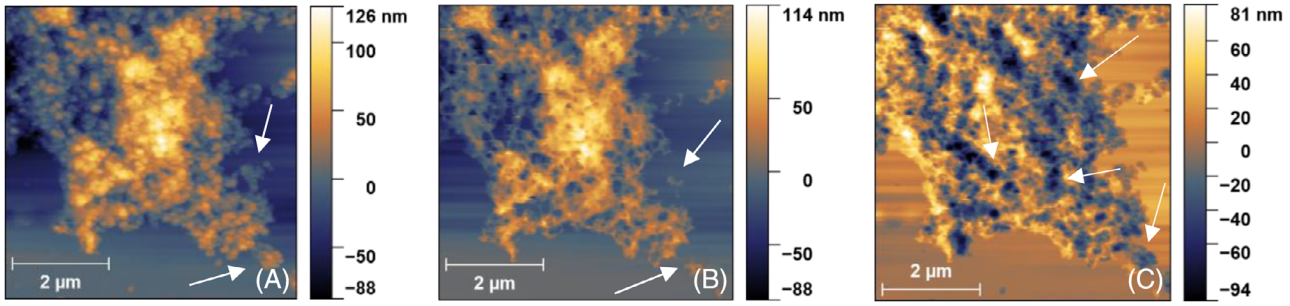

FIGURE 7 AFM images of M-S-H synthesized from a growth solution having [Mg]/[Si] = 1.5 at (A) 0 min and (B) 122 min of dissolution. The difference between the two images is shown in (C), where negative height change indicates dissolution. It can be seen from (C) that the greatest dissolution is observed around the edges where more surface area is exposed. The arrows indicate areas of fastest dissolution, corresponding to surface features such as peaks and valleys. Interior locations in the precipitates showed slower dissolution.

less than 10.[41] Among silicates with no shared O atoms, Mg_2SiO_4 is one of the slowest to dissolve because of the strong hydration of Mg^{2+} ions.[42] The steady-state dissolution rate of C-S-H under far-from-equilibrium conditions has been quantified to be $3.1 \pm 0.4 \times 10^{-11}$ mol/m^2/s,[43] or $3.1 \pm 0.4 \times 10^{-15}$ mol/cm^2/s, which is significantly lower than the dissolution rates measured herein. The low C-S-H dissolution rates can be explained by measurements over much longer durations (433 to 5754 h), wherein the formation of Si-rich domains on C-S-H may significantly inhibit dissolution.[43] Future studies will compare the dissolution rates of M-S-H and C-S-H under equivalent experimental conditions.

The leaching of C-S-H, the primary binding phase in conventional cement systems, is known to occur at pH levels around 10, potentially compromising structural integrity over time.[44] While there is a notable gap in data regarding M-S-H dissolution at similar pH values, the formation of M-S-H has been observed around pH 10 in open-flow systems, implying stability under these conditions.[45] This suggests that M-S-H dissolution is likely to occur at pH < 10 and supports the relevance of the environmental conditions selected in this study. Nonetheless, quantifications of the pH-dependent dissolution rate of M-S-H are critical in understanding phase stability. For instance, an increase in pH from 6 to 10 may result in a reduction in the dissolution rate of M-S-H, similar to other Mg-rich phyllosilicates.[46]

4 | CONCLUSION

Using in situ AFM, we determined the dissolution rates of M-S-H and how its structure influences degradation when exposed to air-saturated water. The phase's morphology significantly affects its dissolution rate, with oriented precipitates featuring up to 10 times faster dissolution rates than non-oriented precipitates. This study suggests that both the chemical reactivity and the spatial arrangement of nanoparticles play crucial roles in controlling the overall dissolution rate. Further investigations are necessary to elucidate the specific mechanisms of M-S-H dissolution and how its mesostructure impacts this process. This study quantifies dissolution rates at early ages. Future research will consider longer durations to identify temporal trends and changes in dissolution behavior. Such studies could provide valuable insights into the long-term stability and behavior of M-S-H-based cements.

ACKNOWLEDGEMENTS

The authors gratefully acknowledge the financial support provided by the National Science Foundation through the CAREER Award #2342381. This work was conducted at the Materials Chemistry Laboratory (MCL), the Center for Advanced Construction Materials (CACM), and the Characterization Center for Materials and Biology (CCMB) at the University of Texas at Arlington and the University of California, Davis. The authors express their appreciation for the support that has facilitated the operations of these laboratories. The contents of this paper represent the views and opinions of the authors, who are responsible for the accuracy of the datasets presented herein. They do not reflect the views and/or policies of the funding agency, nor do the contents constitute a specification, standard, or regulation.

REFERENCES

1. Gagg CR. Cement and concrete as an engineering material: an historic appraisal and case study analysis. Eng Fail Anal. 2014;40:114–40. https://doi.org/10.1016/J.ENGFAILANAL.2014.02.004
2. Gjorv O. E., Sakai K., Concrete Technology for a Sustainable Development in the 21st Century. CRC Press; 1999.
3. Gjørv OE, Gjørv OE. Review article—civil engineering durability of concrete structures. Arab J Sci Eng. 2011;36:151–72. https://doi.org/10.1007/s13369-010-0033-5

4. Perera G, Doremus RH, Lanford W. Dissolution rates of silicate glasses in water at pH 7. J Am Ceram Soc. 1991;74(6):1269–74. https://doi.org/10.1111/J.1151-2916.1991.TB04096.X
5. Lothenbach B, Nied D, L'Hôpital E, Achiedo G, Dauzères A. Magnesium and calcium silicate hydrates. Cem Concr Res. 2015;77:60–68. https://doi.org/10.1016/j.cemconres.2015.06.007
6. Dauzeres A, Achiedo G, Nied D, Bernard E, Alahrache S, Lothenbach B. Magnesium perturbation in low-pH concretes placed in clayey environment—solid characterizations and modeling. Cem Concr Res. 2016;79:137–50. https://doi.org/10.1016/J.CEMCONRES.2015.09.002
7. Brew DRM, Glasser FP. Synthesis and characterisation of magnesium silicate hydrate gels. Cem Concr Res. 2005;35(1):85–98. https://doi.org/10.1016/J.CEMCONRES.2004.06.022
8. Roosz C, Grangeon S, Blanc P, Montouillout V, Lothenbach B, Henocq P, et al. Crystal structure of magnesium silicate hydrates (M-S-H): the relation with 2:1 Mg–Si Phyllosilicates. Cem Concr Res. 2015;73:228–37. https://doi.org/10.1016/J.CEMCONRES.2015.03.014
9. Gunnarsson I, Arnórsson S, Jakobsson S. Precipitation of poorly crystalline antigorite under hydrothermal conditions. Geochim Cosmochim Acta. 2005;69(11):2813–28. https://doi.org/10.1016/J.GCA.2005.02.001
10. Walling SA, Kinoshita H, Bernal SA, Collier NC, Provis JL. Structure and properties of binder gels formed in the system $Mg(OH)_2$ –SiO_2 –H_2O for immobilisation of Magnox sludge. Dalton Trans. 2015;44(17):8126–37. https://doi.org/10.1039/C5DT00877H
11. Zhang T, Cheeseman CR, Vandeperre LJ. Development of low pH cement systems forming magnesium silicate hydrate (M-S-H). Cem Concr Res. 2011;41(4):439–42. https://doi.org/10.1016/J.CEMCONRES.2011.01.016
12. Singh D, Nguyen TTM, Bustamantes E, Wahab A, Yousaf AH, Shortt I, et al. Chemical structure and complex growth modes of magnesium silicate hydrate: nanoparticle orientation, aggregation, and fusion. Cem Concr Res. 2024;175:107367. https://doi.org/10.1016/j.cemconres.2023.107367
13. Oxford Instruments Asylum Research. Liquid perfusion holder for Cypher ES AFM (2024). Asylum Research. https://afm.oxinst.com/products/cypher-operating-in-liquid/cypher-es-liquid-perfusion-cell. Accessed 26 July 2024.
14. Nečas D, Klapetek P. Gwyddion: an open-source software for SPM data analysis. Cent Eur J Phys. 2012;10(1):181–88. https://doi.org/10.2478/S11534-011-0096-2
15. Lammers K, Smith MM, Carroll SA. Muscovite dissolution kinetics as a function of pH at elevated temperature. Chem Geol. 2017;466:149–58. https://doi.org/10.1016/J.CHEMGEO.2017.06.003
16. Nied D, Enemark-Rasmussen K, L'Hopital E, Skibsted J, Lothenbach B. Properties of magnesium silicate hydrates (M-S-H). Cem Concr Res. 2016;79:323–32. https://doi.org/10.1016/j.cemconres.2015.10.003
17. Arvidson RS, Ertan IE, Amonette JE, Luttge A. Variation in calcite dissolution rates: a fundamental problem? Geochim Cosmochim Acta. 2003;67(9):1623–34. https://doi.org/10.1016/S0016-7037(02)01177-8
18. Parkhurst DL, Appelo CAJ. Description of Input and Examples for PHREEQC Version 3A Computer Program for Speciation, Batch-Reaction, One-Dimensional Transport, and Inverse Geochemical Calculations: U.S. Geological Survey Techniques and Methods. 2013.
19. Ueta S, Satoh H, Nishimura Y, Ueda A, Tsukamoto K. Dynamic and topographic observation of calcite dissolution using enhanced in-situ phase-shift interferometry. J Cryst Growth. 2013;363:294–99. https://doi.org/10.1016/j.jcrysgro.2012.11.021
20. Pérez-Garrido C, Fernández-Díaz L, Pina CM, Prieto M. In situ AFM observations of the interaction between calcite ($10\bar{1}4$) surfaces and Cd-bearing aqueous solutions. Surf Sci. 2007;601(23):5499–509. https://doi.org/10.1016/j.susc.2007.09.021
21. Bisschop J, Dysthe DK, Putnis CV, Jamtveit B. In situ AFM study of the dissolution and recrystallization behaviour of polished and stressed calcite surfaces. Geochim Cosmochim Acta. 2006;70(7):1728–38. https://doi.org/10.1016/J.GCA.2005.12.013
22. Pedrosa ET, Kurganskaya I, Fischer C, Luttge A. A statistical approach for analysis of dissolution rates including surface morphology. Minerals. 2019;9(8):458. https://doi.org/10.3390/MIN9080458
23. de Ruiter L, Gunnæs AE, Dysthe DK, Austrheim H. Quartz dissolution associated with magnesium silicate hydrate cement precipitation. Solid Earth. 2021;12(2):389–404. https://doi.org/10.5194/se-12-389-2021
24. Pollet-Villard M, Daval D, Fritz B, Knauss KG, Schäfer G, Ackerer P. Influence of etch pit development on the surface area and dissolution kinetics of the orthoclase (001) surface. Chem. Geol. 2016;447:79–92. https://doi.org/10.1016/j.chemgeo.2016.09.038
25. Saldi GD, Köhler SJ, Marty N, Oelkers EH. Dissolution rates of talc as a function of solution composition, pH and temperature. Geochim Cosmochim Acta. 2007;71(14):3446–57. https://doi.org/10.1016/j.gca.2007.04.015
26. Daval D, Hellmann R, Martinez I, Gangloff S, Guyot F. Lizardite serpentine dissolution kinetics as a function of pH and temperature, including effects of elevated pCO_2. Chem Geol. 2013;351:245–56. https://doi.org/10.1016/j.chemgeo.2013.05.020
27. Pokrovsky OS, Schott J. Kinetics and mechanism of forsterite dissolution at 25°C and pH from 1 to 12. Geochim Cosmochim Acta. 2000;64(19):3313–25. https://doi.org/10.1016/S0016-7037(00)00434-8
28. Lattice dynamics of forsterite. American Mineralogist | GeoScienceWorld. https://pubs.geoscienceworld.org/msa/ammin/article-abstract/63/11-12/1198/40830/Lattice-dynamics-of-forsterite. Accessed 30 Dec 2022.
29. Knauss KG, Wolery TJ. The dissolution kinetics of quartz as a function of pH and time at 70°C. Geochim Cosmochim Acta. 1988;52(1):43–53. https://doi.org/10.1016/0016-7037(88)90055-5
30. Icenhower JP, Dove PM. The dissolution kinetics of amorphous silica into sodium chloride solutions: effects of temperature and ionic strength. Geochim Cosmochim Acta. 2000;64(24):4193–203. https://doi.org/10.1016/S0016-7037(00)00487-7
31. Jordan G, Rammensee W. Dissolution rates and activation energy for dissolution of brucite (001): a new method based on the microtopography of crystal surfaces. Geochim Cosmochim Acta. 1996;60(24):5055–62.
32. Dove PM, Han N, Wallace AF, De Yoreo JJ. Kinetics of amorphous silica dissolution and the paradox of the silica poly-

morphs. Proc Natl Acad Sci. 2008;105(29):9903–8. https://doi.org/10.1073/PNAS.0803798105

33. Luce RW, Bartlett RW, Parks GA. Dissolution kinetics of magnesium silicates. Geochim Cosmochim Acta. 1972;36(1):35–50. https://doi.org/10.1016/0016-7037(72)90119-6
34. Rayner JH, Brown G. The crystal structure of talc. Clays Clay Miner. 1973;21(2):103–14. https://doi.org/10.1346/CCMN.1973.0210206/METRICS
35. Schliemann R, Churakov SV. Atomic scale mechanism of clay minerals dissolution revealed by ab initio simulations. Geochim Cosmochim Acta. 2021;293:438–60. https://doi.org/10.1016/j.gca.2020.10.026
36. Xiao Y, Lasaga AC. Ab initio quantum mechanical studies of the kinetics and mechanisms of silicate dissolution: H+(H_3O+) catalysis. Geochim Cosmochim Acta. 1994;58(24):5379–400. https://doi.org/10.1016/0016-7037(94)90237-2
37. Lin F-C, Clemency CV. The dissolution kinetics of brucite, antigorite, talc, and phlogopite at room temperature and pressure. Am Mineral. 1981;66(7-8):801–6.
38. Brown GE. Olivines and silicate spinels. Rev Mineral Geochem. 1980;5(1):275–381.
39. Lupulescu AI, Rimer JD. In situ imaging of silicalite-1 surface growth reveals the mechanism of crystallization. Science. 2014;344(6185):729–32. https://doi.org/10.1126/science.1250984
40. Zhu G, Legg BA, Sassi M, Liang X, Zong M, Rosso KM, et al. Crystal dissolution by particle detachment. Nat Commun. 2023;14(1):6300. https://doi.org/10.1038/s41467-023-41443-y
41. Bernard E, Lothenbach B, Cau-Dit-Coumes C, Chlique C, Dauzères A, Pochard I. Magnesium and calcium silicate hydrates, part I: investigation of the possible magnesium incorporation in calcium silicate hydrate (C-S-H) and of the calcium in magnesium silicate hydrate (M-S-H). Appl Geochem. 2018;89:229–42. https://doi.org/10.1016/J.APGEOCHEM.2017.12.005
42. Brantley SL. Kinetics of mineral dissolution. In Brantley SL, Kubicki JD, White AF, editors. Kinetics of water-rock interaction. Springer New York: New York, NY; 2008. p. 151–210. https://doi.org/10.1007/978-0-387-73563-4_5
43. Trapote-Barreira A, Cama J, Soler JM. Dissolution kinetics of C-S-H Gel: flow-through experiments. Phys Chem Earth. 2014;70–71:17–31. https://doi.org/10.1016/j.pce.2013.11.003
44. Ma Y, Li W, Jin M, Liu J, Zhang J, Huang J, et al. Influences of leaching on the composition, structure and morphology of calcium silicate hydrate (C–S–H) with different Ca/Si ratios. J Build Eng. 2022;58:105017. https://doi.org/10.1016/j.jobe.2022.105017
45. Bernard E, Lothenbach B, Rentsch D, Pochard I, Dauzères A. Formation of magnesium silicate hydrates (M-S-H). Phys Chem Earth Parts ABC. 2017;99:142–57. https://doi.org/10.1016/j.pce.2017.02.005
46. Schott J, Pokrovsky OS, Oelkers EH. The link between mineral dissolution/precipitation kinetics and solution chemistry. Rev Mineral Geochem. 2009;70(1):207–58. https://doi.org/10.2138/rmg.2009.70.6

How to cite this article: Wahab A, Nguyen TTM, Singh D, La Plante E. Dissolution kinetics of cementitious magnesium silicate hydrate in air-equilibrated water. J Am Ceram Soc. 2024;107:8547–55. https://doi.org/10.1111/jace.20102